[20] —, "Architektur aus dem Meer," *Deutsche Bauzeit*, vol. 11, no. 5, p. 14, 1977.
[21] —, "Minimal-Maximal-Strukturen aus Meerwasser," in: *Minimal-Konstruktionen*, E. Bubner, B. Baier, R. Koenen and J. Oelbermann, Eds. Köln-Braunsfeld, Germany: Verlagsgesellschaft Rudolf Müeller, 1977, pp. 191–203.
[22] W. H. Hilbertz, D. Fletcher, and C. Krausse, "Mineral accretion technology: Applications for architecture and aquaculture," *Indust. Forum*, vol. 8, no. 4–5, pp. 78–84, 1977.
[23] L. Edmond, "Marine habitat improvement in Japan," *Foreign Service Dispatch No. 180*, American Embassy, Tokyo, U.S. Dep. State, Washington, DC, pp. 1–4, Aug. 1960.
[24] R. B. Stone, C. C. Buchanan, and R. O. Parker, Jr., "Expansion and evaluation of an artificial reef off Murrells Inlet, SC," Final Rep., to Atlantic Estuarine Fisheries Center, National Marine Fisheries Service, U.S. Dep. Commerce, Beaufort, NC, 1973.
[25] R. H. Strand and W. H. Massman," Artificial reefs as tools of sport fishery management in coastal marine waters," *SFI Bull.*, no. 170, pp. 1–8, Jan. 1966.
[26] J. Arne, "Preliminary report on attracting fish by oyster shell plantings in Chincoteague Bay, Mayland," *Chesapeake Sci.*, vol. 1, no. 1, pp. 58–65, 1960.
[27] H. T. Kami, "Studies on effect of shelter on standing crop of fishes," *Job Completion Rep.*, U.S. Fish and Wildlife Service, HI, F-5-R-F (Job 10), 1959 (unpublished manuscript).
[28] C. H. Turner, "A study of artificial reefs," presented at the 5th Annu. Conv. Underwater Society of America, Mexico, June 18–20, 1964.
[29] D. P. DeSylva, "Base for reef," *SFI Bull.*, no. 12, pp. 4–5, Apr. 1962.
[30] H. B. Olin, *Construction*. Chicago, IL: Inst. Fin. Education, Sec. 203-3, 1975.

Passive Systems Theory With Narrow-Band and Linear Constraints: Part III—Spatial/Temporal Diversity

JOSÉ M. MOURA

Abstract—**This is the last of a series of three papers studying the theory of passive systems. The model assumes that i) the narrow-band signals are transmitted through a Rayleigh channel, ii) the observing array is geometrically linear, and iii) the source motion is deterministic. Ranging techniques based on synchronized measurements of the travel time delay are precluded by the incoherent phase model considered. The paper explores alternative methods that process the phase modulations induced on the signal by the extended geometry and relative dynamics. The present work applies maximum likelihood theory to design the receiver, being concerned with the global identifiability of all parameters defining the relative source/receiver geometry and dynamics. The emphasis is placed on the passive range global acquisition.**

In contradistinction with the previous papers, where the time stationarity (Part I) or the space homogeneity (Part II) lead to a one-dimensional processor, here the receiver involves processing over both domains. The paper considers the issues of space/time factorability and coupling arising in nonhomogeneous passive tracking. The cross coupling, resulting in more complex filters, improves the receiver acquisition capability. Resorting to Taylor's series type studies, the paper quantifies these improvements, as well as the receiver's mean square error performance, in terms of intuitively satisfying analytical expressions.

I. INTRODUCTION

THE PAPER is the last one of a series of three (see [1], [2]), studying the passive tracking of a source by processing its radiated signature (e.g., propeller's noise). These problems arise in several contexts of practical significance, here classified in two groups:

i) positioning problems (Fig. 1(a)), where the interest lies on locating the source;
ii) navigation problems (Fig. 1(b)), where a string of beacons (or a moving satellite) is used as a navigational reference.

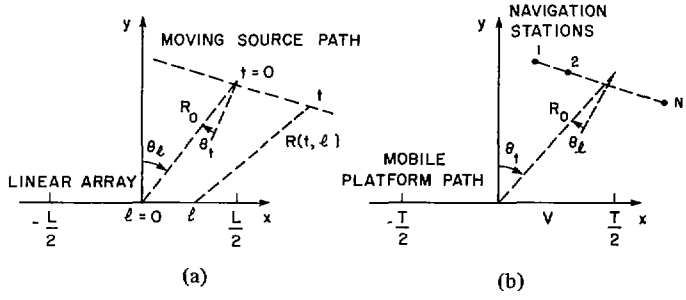

Fig. 1. Passive tracking positioning/navigation applications. (a) Positioning. (b) Navigation.

The reader is referred to Parts I [1] and II [2] for a brief discussion on these and other applications of the passive tracking theory. Here, the analysis is focused on the passive positioning context.

Fig. 1(a) illustrates the basic problem configuration. A moving source of unknown position is to be tracked by an array of sensors. The space extent of the receiver's array (spatial diversity) and the time baseline of the source travel (temporal diversity) modulate nonlinearly the radiated signal. The problem is the determination of the relative geometry and dynamics by processing the structure induced on the signal.

Manuscript received December 1, 1978; revised April 21, 1979. This work was carried out at the M.I.T. Research Laboratory of Electronics, Cambridge, MA. This work was supported in part by the Joint Services Electronics Program under Contract DAAB07-71-C-0300.

The author is with the Centro de Análise e Processamento de Sinais, Complexo Interdisciplinar and the Department of Electrical Engineering, Instituto Superior Técnico, Av. Rovisco Pais, 1000 Lisboa, Portugal.

0364-9059/79/0700-0113$00.75 © 1979 IEEE

The previous papers [1], [2] introduced a homogeneity in one of the time/space domains. Part I considered a fixed source, while Part II assumed an omnidirectional receiving aperture. These constraints lead to a simpler problem where only one of the time/space aspects is relevant. This work studies passive tracking situations where both spatial and temporal nonnegligible baselines are generated. The signal's wavefront has a coupled structure, exhibiting simultaneous spatial curvature and temporal modulation.

In Section II, we establish the model, by constraining the geometry, the dynamics, the signals, and the statistical aspects of the problem. In Section III, we present the maximum-likelihood (ML) receiver, while in Sections IV and V, we analyze its structure and its performance for two practically important configurations. In Section VI, we summarize the basic conclusions of the work. Keeping the positioning terminology introduced in Parts I and II, the class of problems dealt with herein is referred to as a Stationary Array/Moving Source (SAMS) application.

II. MODEL

The assumptions in Parts I [1] and II [2] of a planar geometry, narrow-band radiated signals, linear array structures, and deterministic constant speed linear dynamics are kept. In connection with Fig. 1, the range function $R(t, l)$ is the distance between the source at time t and the point at location l in the linear array. Under the deterministic assumptions on the motions, $R(t, l)$ may be completely described by four parameters. Centering the relative geometry with respect to the array center and the midpoint of the observation interval, the parameter vector is defined

$$A = [R_0 v \sin\theta_t \sin\theta_l]^T \tag{1}$$

where $[\cdot]^T$ stands for vector transposition, R_0 is the source/receiver separation at $t = 0$, $l = 0$, angles $\sin\theta_i$, $i = t, l$ are indicated in Fig. 1, and v is the source speed. The range function[1]

$$R(t, l, A) \triangleq R(t, l) = \{R_0^2 + l^2 + (vt)^2 - 2R_0(l\sin\theta_l + vt\sin\theta_t) + 2lvt\cos(\theta_l - \theta_t)\}^{1/2} \tag{2}$$

or equivalently,

$$R(t, l, A) = \{[R_0 - l\sin\theta_l - vt\sin\theta_t]^2 + [l\cos\theta_l + vt\cos\theta_t]^2\}^{1/2}. \tag{3}$$

The received signal

$$r(t, l) = \sqrt{2}\ \mathrm{Re}\ \{\tilde{r}\exp j\omega_c t\} \tag{4}$$

where the complex amplitude

$$\tilde{r} = \tilde{s} + \tilde{w}. \tag{5}$$

[1] As in Parts I and II t, l, and A will usually be omitted from the functions's list of arguments.

The measurement noise $\tilde{w}$ is a zero mean, spatially and temporally "white" Gaussian noise with double spectral height of N_0. The signal complex envelope

$$\tilde{s} = \sqrt{E_r}\,\tilde{b}\,\tilde{s}_n \tag{6}$$

with $\tilde{s}_n$ the normalized version

$$\tilde{s}_n(t, l, A) = \frac{1}{\sqrt{LT}}\exp\left\{-j\frac{2\pi}{\lambda}R(t, l, A)\right\}. \tag{7}$$

In these equations, $E_r = PLT$ = total energy received during the observation interval $[-T/2, T/2]$; P = signal power; L = array length; $\lambda = c/f$ = wavelength; $\tilde{b} = b\exp j\psi$, with b Rayleigh, and ψ uniformly distributed random variables. The zero-mean Gaussian random variable $\tilde{b}$, with variance $2\sigma_b^2$, is independent of $\tilde{w}(t, l)$. Besides measuring model inaccuracies, $\tilde{b}$ precludes the passive determination of the range from the synchronous observation of the constant travel time delay [3], see related remark in Part II [2].

Note that the model works with $\sin\theta_i$, $i = l, t$ and not with the angles themselves. This does not specify uniquely the angles θ_i in $(-\pi, \pi)$. It is the usual ambiguity cone, characteristic of linear arrays. To illustrate the point, consider a ship navigation problem. Then, either it is known the side where the source center is or the experiment has to be repeated with a different line course.

The subsequent analysis will make use of the following geometry parameters:

$$X_l = L/2R_0 \qquad \text{and} \qquad X_t = vT/2R_0. \tag{8}$$

They normalize with respect to the source/receiver separation the linear dimensions (half of the array length, or half of the source travel).

III. RECEIVER STRUCTURE

The passive positioning/navigation application with spatial and temporal diversity has been cast in the context of an estimation problem with a finite number of nonrandom unknown parameters. These are imbedded nonlinearly on signals corrupted by a multiplicative random quantity (Rayleigh channel) and by an additive (temporally white, spatially homogeneous) Gaussian noise. The ML estimation theory [4] is now applied to derive the asymptotically efficient ML-receiver. The processor is a matched filter followed by a square law envelope detector. The ML-receiver maximizes the log ML-function, the structure of which is determined by the signal correlation

$$\psi(A, \bar{A}) = \langle \tilde{s}_n(A), \tilde{s}_n(\bar{A})\rangle \triangleq \int_{-T/2}^{T/2} dt \int_{-L/2}^{L/2} dl\, \tilde{s}_n(A)\tilde{s}_n^*(\bar{A}) \tag{9}$$

and by the Generalized Ambiguity Function (GAF)

$$\Phi(A, \bar{A}) = |\psi(A, \bar{A})|^2. \tag{10}$$

In these expressions A stands for the actual source parameter vector and $\bar{A}$ for the scanning value over Ω. For details see [1] and [2].

Equations (9) and (10) describe a processing over two dimensions; space and time. In Parts I and II, the homogeneity introduced in one of these domains (the time stationarity of the relative dynamics in Part I or the omnidirectional sensor in Part II) lead to a simpler one-dimensional filter. This stationarity can be viewed as a special case of the more general one where the receiver's structure is decoupled, i.e., where

$$\psi(A, \bar{A}) = \psi_l(A, \bar{A})\psi_t(A, \bar{A}). \tag{11}$$

In (11) $\psi_i(A, \bar{A}), i = l, t$ are one-dimensional integrals. The importance of (11) is twofold. First, it expresses the filter in terms of two independent blocks, each representing an operation in a single domain. If there are changes in one of them not affecting the assumptions underlying the factorability (11), the block in the other domain is left unaltered. Second, (11) may lead to separability *over the parameter space* Ω of the signal autocorrelation, and hence of the generalized ambiguity function, giving rise to considerable savings in the processing load work.[2]

The present SAMS model exhibits no homogeneity in either of the space/time domains, so that in general factorability (11) does not occur. The direct analysis of the receiver is not conducive to intuitively interpretable expressions. Numerical and graphical studies, as done in Parts I and II, could be pursued. Here, however, attention is turned to two configurations illustrating two basic questions. The first, studied in Section IV, assumes that the temporal diversity dominates the spatial diversity, leading to a receiver presenting, for all practical purposes, a decoupled structure. The SAMS problem can be put in the perspective of the simpler reduced-dimension problems of Parts I and II. The second, analyzed in Section V, considers comparable temporal and spatial baselines, assessing how the space/time coupling affects the receiver and its performance. In both sections, a least order analysis, based on truncated Taylor's series approximations, is pursued.

IV. DECOUPLED SPATIAL/TEMPORAL SAMS STRUCTURE

This section considers the limiting configuration where the receiver's array length is much smaller than the observed source travel. The following two hypotheses are made concerning the geometric configuration of SAMS:

$$X_l = L/2R_0 \ll 1 \tag{12a}$$

$$X_l \ll X_t = vT/R_0. \tag{12b}$$

Note that (12a) corresponds to a distant (spatial) source/observer configuration, justifying a linearized Taylor's series analysis on the spatial variable. The range function becomes

$$R(t, l) \approx R(t, 0) + \frac{\cos(\theta_t - \theta_l)vt - R_0 \sin\theta_l}{R(t, 0)} l \tag{13a}$$

$$= R(t, 0) - \sin\theta_l(t, 0) \tag{13b}$$

where $\theta_l(t, 0)$ is the bearing angle at time t with respect to the center of the reference frame. This linearized structure in the space variable states that, at each particular instant of time, the wave field across the receiver's array is planar, and that, as the source moves along its linear track, the spatial structure of the received signal changes. Note that $R(t, 0)$ depends only on the reduced dimension vector

$$A_0 = [R_0 v \sin\theta_t]^T \tag{14}$$

associated with the Stationary Array/Moving Source with omnidirectional sensor ($SAMS_o$) model of Part II [2]. In (14), as before, $[\cdot]^T$ stands for vector transposition.

A. Ambiguity Structure

Since, instantaneously, the wavefronts are planar across the array, spatial diversity techniques (array processing with beam forming) are used to match the bearing angle. As the source sweeps the horizon, the receiver updates the bearing estimate. Substituting (13) in (7) and (9), it can be shown [8] that the receiver's structure practically decouples. The signal autocorrelation becomes approximately

$$\psi(A, \bar{A}) \cong \psi_t(A_0, \bar{A}_0)\psi_l(\Delta \sin\theta_l(t, 0, A, \bar{A})). \tag{15}$$

In (15) $\psi_t(A_0, \bar{A}_0)$ is the signal autocorrelation associated with the $SAMS_o$ problem of Part II [2], while

$$\psi_l(\Delta \sin\theta_l(t, 0, A, \bar{A}))$$

$$= \operatorname{sinc}\left[\frac{2\pi}{\lambda}\Delta \sin\theta_l(t, 0, A, \bar{A})\frac{L}{2}\right] \tag{16a}$$

where

$$\Delta \sin\theta_l(t, 0, A, \bar{A}) = \sin\theta_l(t, 0, A) - \sin\theta_l(t, 0, \bar{A}). \tag{16b}$$

Steering the array, see Fig. 2, as the source travels through, the function $\psi_l(\cdot)$ is kept practically tuned to 1. The spatial bearing θ_l is sequentially updated. To compute the number of updates N_u define the array bearing resolution [9] by the bearing interval over which the (spatial) aperture response does not drop below the 3-dB cutoff, i.e., by

$$\psi_l \sin\theta_l(t_1, 0) - \sin\theta_l(t_2, 0)) > \frac{1}{\sqrt{2}}. \tag{17a}$$

[2] In the detection context a different concept of factorability is considered [5], see also [6] and [7]. Therein, the receiver separates in two operations, one dependent on the geometry and the other on the noise statistics. It has already been noted (see [1, Section VII]) that the signal model (4)-(7) considered here leads to a receiver where the geometry and statistical aspects are decoupled.

[3] $\operatorname{sinc} X = \sin X/X$

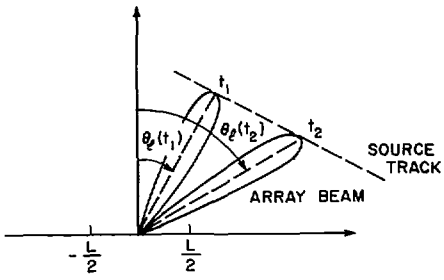

Fig. 2. Sequential beam steering.

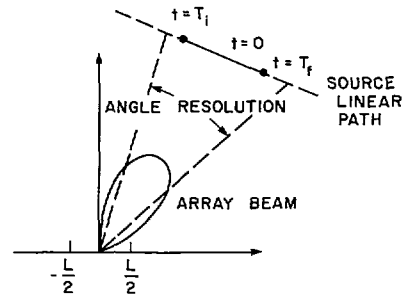

Fig. 3. Source dynamics within a resolution cell of the linear array.

Since $\psi_l(\cdot)$ is the sinc function of (16a) and taking $t_1 = 0$ in (17a), the resolution is

$$\Delta \sin\theta_l = \sin\theta_l - \sin\theta_l(t_2, 0) < 2.78/(2\pi/\lambda)L. \tag{17b}$$

The total bearing variation across the source travel is approximately

$$\sin\theta_l\left(\frac{T}{2}, 0\right) - \sin\theta_l\left(-\frac{T}{2}, 0\right) \approx 2\cos(\theta_l - \theta_t)X_t \tag{17c}$$

so that the number of updates is

$$N_u \cong \left\lfloor 4.5\cos(\theta_l - \theta_t)\frac{LX_t}{\lambda} \right\rfloor \tag{17d}$$

where $\lfloor(\cdot)\rfloor$ stands for the largest integer contained in $(\cdot)$. In particular, for a parallel geometry ($\theta_l = \theta_t$),

$$N_u \cong 2.25(L/\lambda)(vT/R_0). \tag{17e}$$

Defining the total number of λ-range cells at $l = 0$, as

$$N_\lambda = \lfloor R_0/\lambda \rfloor \tag{17f}$$

(17c) becomes

$$N_u \cong 9X_lX_tN_\lambda. \tag{17g}$$

When $N_u = 1$ the signal autocorrelation (15) is

$$\psi(A, \bar{A}) = \psi_0(A_0, \bar{A}_0)\,\mathrm{sinc}\left[\frac{2\pi}{\lambda}(\Delta\sin\theta_l)\frac{L}{2}\right] \tag{18}$$

i.e., it factors as the product of the signal autocorrelation functions associated respectively with the $\mathrm{SAMS_o}$ configuration of Part II and with the Synthetic Observer/Stationary Source (SOSS) problem of Part I. This says that, when the angle spanned by the source travel is within the receiver's aperture beamwidth (Fig. 3) the SAMS signal autocorrelation decouples in its spatial and temporal aspects. To this space/time decoupling there corresponds a factorization over the parameter space Ω, with a significant reduction of the computational effort involved in the ML-receiver.

When $N_u > 1$, the sequential beam steering technique of Fig. 2 still leads to the decoupled autocorrelation (15). The receiver has a cascaded block structure. Its tuning is accomplished by scanning independently the bearing angle (space diversity) and the A_0 parameter vector (time diversity). The range is passively estimated by processing the temporal modulations, while the receiver yields a sequence of bearing measurements instead of a single bearing estimate.

B. Mean-Square Performance

The analysis concentrates on the mean-square spread matrix M, given in Parts I [1] and II [2]. It represents the coefficient matrix of the quadratic form defining the elipsoidal main lobe of (10). This matrix inverse M^{-1} exhibits how the geometric aspects of the problem are reflected on the ML–estimation mean square error performance. In fact, for example, the Cramer-Rao inequality [4], bounds the covariance of the errors Λ_ϵ by

$$\Lambda_\epsilon > [GM]^{-1} \tag{19a}$$

with the gain G dependent on the signal-energy-to-noise ratio, see [1].

By a continuity argument it can be shown, see [8], that, for sufficiently short baseline arrays

$$M^{-1} = \left[\begin{array}{c|c} M_0^{-1} & m \\ \hline m^T & \left(M_{44_{\theta_l}}\dfrac{X_l^2}{3}\right)^{-1} \end{array}\right] \tag{19b}$$

where $m = -M_{44_{\theta_l}}^{-1} M_0^{-1} m$, M_0 is the mean-square spread matrix associated with the $\mathrm{SAMS_o}$ model of Part II [2]

$$\left(M_{44_{\theta_l}}\frac{X_l^2}{3}\right)^{-1} \xrightarrow[X_l \to 0]{} 3(\lambda/\pi L)^2 \tag{19c}$$

and m is of no concern to the present analysis, see [8] for further details. Equation (19) represents M^{-1} for SAMS, when, due to the overall geometry, the signal wavefront is instantaneously planar across the array. Range focussing, as well as

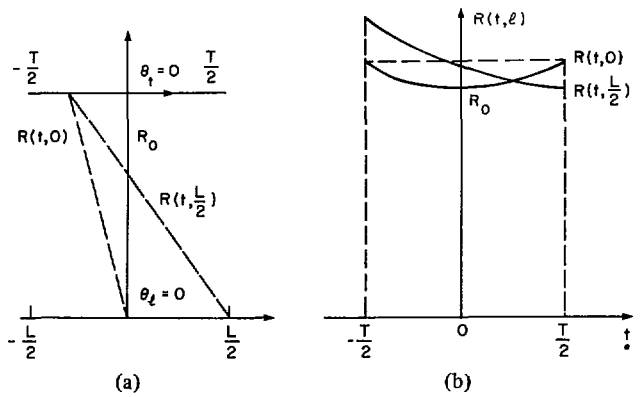

Fig. 4. Spatial/temporal cross coupling ($X_l = X_t$). (a) Geometry. (b) Range function.

estimation of v and $\sin\theta_t$, result from the processing of the temporal modulations. The global and local mean-square performance results of Part II remain then applicable. The spatial bearing is observed from the spatial diversity structure: up to least order effects, the performance results corresponding to the "bearings only" problem apply.

V. COUPLED SPATIAL/TEMPORAL SAMS STRUCTURE

This section studies the problem where the spatial/temporal structures are coupled. The source travels in the near field of the array, being observed by the receiver for a sufficiently large time interval. Significant (spatial) curvature and higher order (temporal) modulation effects are available, see Fig. 4, to yield the estimation of the four source parameters. The range function $R(t, l)$ exhibits a significant variation at each instant across the linear array, and at each array point across the source travel, as Fig. 4 illustrates for a broadside ($\theta_l = 0$)/closest approach ($\theta_t = 0$) geometry.

To obtain an intuitive understanding of the coupling issues, the analysis is pursued when

$$X_l = L/2R_0 < 1 \tag{20a}$$

$$X_t = vT/2R_0 < 1. \tag{20b}$$

These conditions justify a higher order truncated Taylor's series study in both space and time variables about the geometry center $t = 0, l = 0$.

The range function can be written as

$$R(t, l, A) + R(0, 0, A) \cong R_t + R_l + R_{lt} \tag{21a}$$

where R_t, R_l stand for truncated Taylor's series expansions of $R(t, 0, A)$ and $R(0, l, A)$, respectively. In (21a) R_{lt} is the cross coupling term whose lowest order approximation is

$$R_{lt} \approx \frac{[\cos\theta_l l][\cos\theta_t(vt)]}{R_0}. \tag{21b}$$

Due to the incoherent phase model (Rayleigh channel), the term $R_0 = R(0, 0, A)$ in (21a) may be incorporated in the unknown signal absolute phase reference. Since it plays no role on the phase estimation problem it is ignored in the sequel.

A. Ambiguity Structure

Using (21) as an approximation to the range, the signal autocorrelation function can be rewritten as

$$\psi(A, \bar{A}) = \psi_s(A_s, \bar{A}_s)\psi_0(A_0, \bar{A}_0) + J_{lt} \tag{22a}$$

where $\psi_s(\cdot, \cdot)$ and $\psi_0(\cdot, \cdot)$ are the signal autocorrelations associated with SOSS and SAMS_0 of Parts I and II

$$A_s = [R_0 \sin\theta_l]^T \tag{22b}$$

and J_{lt} exhibits the coupled nature of the processor. This term involves the double integration in time and space of a highly nonlinear function, its expression being quite complex.

In [8], by exploiting the harmonic nature of the integrand, the method of stationary phase (see for example [10]) is applied to discuss the asymptotic behavior and rate of falloff of the ambiguity structure. Also (22a) is studied there for specific subspaces of the parameter space Ω. The effect of the coupling can be summarized as sharpening the ambiguity structure while maintaining the fundamental aspects, already observed in Parts I and II, namely: the existence of a main lobe with negligible subsidiary peaks. The quantitative analysis of this main lobe is pursued on Section V-B.

Due to its relevance and simplicity, the ambiguity function expression along the range parameter R_0 is considered. By defining a change of variables, the double integration can be reduced to a single one, leading to

$$\psi(A, \bar{A}) = \frac{(X_{lc} + X_{tc})^2}{X_{lc}X_{tc}}\psi'(A, \bar{A}) \tag{23a}$$

with

$$\psi(A, \bar{A}) = \frac{1}{X_{lt_c}}\int_0^{X_{lt_c}} \left(1 - \frac{2\sigma}{X_{lt_c}}\right) \cdot \exp\left[j(\Delta K)\sigma^2\right] d\sigma \tag{23b}$$

where

$$X_{lc} = \frac{L}{2R_0}\cos\theta_l = \frac{L_{lc}}{R_0} \tag{23c}$$

$$X_{t_c} = \frac{vT}{2R_0}\cos\theta_t = \frac{L_{tc}}{R_0} \tag{23d}$$

$$X_{lt_c} = 2(X_{l_c} + X_{t_c}) \tag{23e}$$

$$\Delta K = \pi(1/R_0 - 1/\bar{R}_0)/\lambda. \tag{23f}$$

Equation (23b) shows the spatial/temporal coupled signal autocorrelation along the radial parameter subspace. It involves a single integration. Apart a normalizing factor, it corresponds to the signal autocorrelation for a particular one-dimensional problem: the source is at broadside condition,

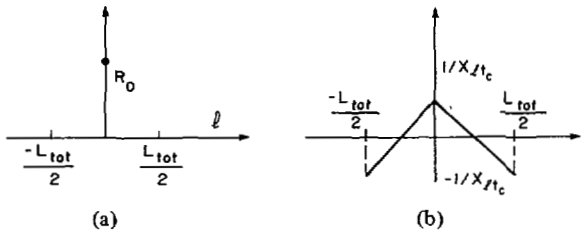

Fig. 5. Equivalent one-dimensional problem. (a) Equivalent SOSS problem. (b) Triangular shading.

the equivalent total linear array extent is, see Fig. 5(a),

$$L_{tot} = L\cos\theta_l + vT\cos\theta_t \tag{23g}$$

and the array shading is not uniform but triangular, as illustrated in Fig. 5(b).[4] When, with the exception of R_0, all the source parameters, are known, (23g) shows that the acquisition at endfire ($\theta_l = \pi/2$) of a source moving radially ($\theta_t = \pi/2$) leads to difficulties.

B. Mean-Square Performance

The mean-square error performance analysis is carried out by resorting to Taylor series developments. Restricting attention to the lowest order terms of the diagonal elements of M^{-1}, one can see [8]

$$M_{R_0}{}^{-1} = (M^{-1})_{11} = \left(\frac{\lambda}{2\pi}\right)^2 \frac{3^2\cdot 5}{X_{c_l}{}^4}\,\frac{1+(4/5)\gamma^2}{1+(4/5)\gamma^2+\gamma^4} \tag{24a}$$

$$M_v{}^{-1} = (M^{-1})_{22} = \left(\frac{\lambda}{2\pi}\right)^2 \frac{v^2}{R_0{}^2} \cdot \frac{3^2\times 5\cos^2\theta_t}{\cos^2\theta_l X_l{}^2 X_t{}^2}\,\frac{1+5\gamma^2+\gamma^4}{5+4\gamma^2+5\gamma^4} \tag{24b}$$

$$M_{\sin\theta_t}{}^{-1} = (M^{-1})_{33} = M_v{}^{-1}\left(\frac{\sin\theta_t}{v}\right)^2 \tag{24c}$$

$$M_{\sin\theta_l}{}^{-1} = (M^{-1})_{44} \approx \left(\frac{\lambda}{2\pi}\right)^2 \frac{1}{R_0{}^2}\,\frac{3}{X_l{}^2} = \left(\frac{\lambda}{2\pi}\right)^2 \frac{12}{L^2}. \tag{24d}$$

In the preceding equations

$$\gamma = \frac{X_{c_t}}{X_{c_l}} = \frac{vT\cos\theta_t}{L\cos\theta_l} \tag{24e}$$

[4] Notice that (23b) generalizes the usual one-dimensional distribution of the (Fresnel zone) diffracted field for a plane wave in optics, to the case where the line source (equivalent in the SAMS problem to the temporal baseline) and the receiving aperture (spatial baseline) are not parallel ($\theta_l \neq \theta_t$), and there is a wide angle ($\theta_l \neq 0$) and oblique incidence ($\theta_t \neq 0$), see for example [10].

defines the realtion between the temporal and spatial effective baselines, as seen from the oblique angle θ_t and bearing θ_l.

Equations (24a), (24b), and (24c) show that these inverse diagonal elements are of fourth order in X_l and X_t. They represent an improvement of order two over the decoupled problem performance of Section IV. In that section, the corresponding results are the $SAMS_o$ ones, whose first nonzero term is of order $X_t{}^{-6}$ (see Part II). It is concluded that the spatial/temporal cross coupling improves, in a nontrivial way, the joint estimation of all source parameters, reducing the overall order of the problem. Intuitively speaking, with the decoupled problem (see Section IV and Part II), at least third-order temporal effects are required for the estimation problem to be nonsingular. The cross coupling, on the other hand, reduces to second the least order effects that have to be measured.

To provide an interpretation for the above results, a comparison between them and the ones in Parts I and II is made. Three particular geometric configurations are considered. Since (24d) equals the corresponding expression for the decoupled problem, the discussion concentrates on the range and speed inverse mean-square spread.

1) Spatial Baseline Much Larger than Temporal Baseline: If

$$\gamma \ll 1 \tag{25a}$$

then

$$(M_{R_0}{}^{-1})_{\rm I} \approx \left(\frac{\lambda}{2\pi}\right)^2 \frac{3^2\times 5}{X_{c_l}{}^4} \approx (M_{R_0}{}^{-1})_{\rm SOSS} \tag{25b}$$

$$(M_v{}^{-1})_{\rm I} \approx \left(\frac{\lambda}{2\pi}\right)^2 \frac{v^2}{R_0{}^2}\,\frac{3^2\times 5\cos^2\theta_t}{\cos^2\theta_l X_l{}^2 X_t{}^2}. \tag{25c}$$

For this geometry the range parameter is estimated from the spatial curvature effects observed across the array.

2) Comparable Spatial and Temporal Baselines: If

$$\gamma = 1 \tag{26a}$$

normalizing with respect to (25b) and (25c), one obtains

$$\frac{(M_{R_0}{}^{-1})_{\rm II}}{(M_{R_0}{}^{-1})_{\rm I}} \approx \frac{9}{14} \tag{26b}$$

which shows that the cross coupling reduces the range standard deviation to approximately 80 percent. Similarly

$$\frac{(M_v{}^{-1})_{\rm II}}{(M_v{}^{-1})_{\rm I}} \approx 2.5. \tag{26c}$$

3) Temporal Baseline Much Larger than Spatial Baseline: If

$$\gamma \gg 1 \tag{27a}$$

normalizing now with respect to the corresponding $SAMS_o$ result

$$\frac{(M_{R_0}{}^{-1})_{III}}{(M_{R_0}{}^{-1})_{SAMS_o}} \approx \frac{X_{t_s}{}^2\gamma^2}{5} \tag{27b}$$

where $X_{t_s} = X_t \sin\theta_t = VT/2R_0 \sin\theta_t$. For the speed v, normalizing with respect to (25c),

$$\frac{(M_v{}^{-1})_{III}}{(M_v{}^{-1})_I} \approx 1. \tag{27c}$$

Expression (27b) states that, for closest approach type geometries ($\theta_t \approx 0°$), for which the range $SAMS_o$ performance decreased sharply, see Part II [2], the coupled structure attains significantly smaller range mean-square errors.

The parameter error cross correlations, as computed from the elements of M^{-1}, are algebraically complex expressions. The reader is referred to [8] where Taylor's series developments and graphical displays are presented for several situations. As examples of the expressions to be found, one has, for a parallel geometry ($\cos\theta_t = \cos\theta_l$) and when $X_t{}^2 = 0.1$ that the cross correlation between the range and speed parameters is

$$\rho_{R_0,v} \approx (2 + 100X_l{}^2 + 1250X_l{}^4)/(2 + 125X_l{}^2 + 1450X_l{}^4 + 2500X_l{}^6). \tag{28a}$$

For a parallel and symmetric ($X_l = X_t$) geometry a Taylor's expansion leads to

$$\rho_{v,\sin\theta_t} \approx -1 + \left[\frac{\sin^2\theta_l + 28}{5} + 891\sin\theta_l{}^4 - 465\cos^2\theta_l\sin^2\theta_l\right]X_l{}^2. \tag{28b}$$

The preceding relations illustrate the high correlations that may exist between parameter errors. On the other hand, (28a) shows that the time/space coupling may reduce the range/speed correlation.

VI. CONCLUSION

This paper has considered positioning/navigation applications when both spatial and temporal diversity are present. After a brief description of the model and receiver, two main classes of problems were pursued. The first was characterized by the dominance of the temporal over the spatial baseline. It was shown that this dominance lead to a decoupled processing structure: the ML-receiver constructs a sequence of bearing angle estimates by processing the spatial delays, while the remaining parameters are estimated from the temporal modulations. The SAMS receiver reduced to a bearings updating scheme (beam former) followed by the $SAMS_o$ processor of Part II [2]. The required number of beam steering updates is given by (17). The second class assumed a balanced geometry, leading to a coupled receiving structure. The cross-coupling term was isolated, its effects analyzed for several limiting geometries. It was concluded that the cross coupling represented a nontrivial improvement, with a decrease of two on the order of the overall problem. The geometry effects on the mean-square performance were assessed, by presenting intuitively satisfying analytical expressions for the inverse of the mean-square spead matrix M. In [11], [12] several applications to positioning and navigation problems of the present theory are considered.

REFERENCES

[1] J. M. F. Moura and A. B. Baggeroer, "Passive systems theory with narrowband and linear constraints. Part I: Spatial diversity," *IEEE Trans. Ocean Eng.*, vol. OE-3, no. 1, Jan. 1978.

[2] —, "Passive systems theory with narrowband and linear constraints. Part II: Temporal diversity," *IEEE Trans. Ocean Eng.*, vol. OE-4, no. 1, Jan. 1979.

[3] L. S. Cahoon and M. J. Hinich, "A method for locating targets using range only," *IEEE Trans. Inform. Theory*, vol. IT-22, pp. 217–225, Mar. 1976.

[4] H. L. Van Trees, *Detection, Estimation and Modulation Theory: Part III.* New York: Wiley, 1971.

[5] D. Middleton and H. L. Groginsky, "Detection of random signals by receivers with distributed elements: Optimum receiver structures for normal signals and noise fields," *J. Acoust. Soc. Amer.*, vol. 38, pp. 727–737, 1965.

[6] H. Urkowitz, C. A. Hauer and J. F. Koval, "Generalized resolution in radar systems," *Proc. IRE*, vol. 50, pp. 2093–2105, 1962.

[7] S. Pasupathy and A. N. Venetsanopoulos, "Optimum active array processing structure and space/time factorability," *IEEE Trans. Aerosp. Electron. Syst.*, vol. AES-10, no. 6, pp. 770–778, Nov. 1974.

[8] J. M. F. Moura, "Passive systems theory with applications to positioning and navigation," Res. Lab. Electron. M.I.T., MA, Rep. 490, Apr. 1976.

[9] A. B. Baggeroer, "Space/time random processes and optimum array processing," NUC Rep. 1973.

[10] A. Papoulis, *Systems and Transforms with Applications in Optics.* New York: McGraw-Hill, 1967.

[11] J. M. F. Moura, "A navigation system for air traffic precision landing," in *Proc. 7th Symp. Signal Processing and Its Applications* (Colloque GRETSI de Nice), May 28–June 2, 1979.

[12] —, "Platform location in underwater acoustics," in *Proc. IEEE Conf. Oceans 1979* (San Diego, CA), Sept. 17–19, 1979.